CORRECTED 30 SEPTEMBER 2011; SEE LAST PAGE

binding site (fig. S8A and fig. S9), Get1 must displace helix $\alpha2^{Get2}$, which is connected to helix $\alpha1^{Get2}$ by the flexible glycine linker. NMR analyses revealed that Get1 binding indeed causes some Get2 interactions with Get3 to disappear. Specifically, interaction with Get2 was observed in the region of L4 to A49, and upon addition of Get1, residues G24 to A49 no longer interacted with Get3 (fig. S10). This shows that helix $\alpha2^{Get2}$ is no longer bound to Get3 in the ternary complex.

On the basis of different crystal structures of Get3, we previously proposed a model for how the Get3 ATPase regulates TA protein insertion (*19*). With structures of different Get3-receptor complexes as well as functional data in hand, distinct docking states can be integrated into this model (Fig. 4). Assisted by Get4/5/Sgt2, TA proteins bind to Get3-ATP-Mg^{2+} (step 1). After ATP hydrolysis, the reaction products stay trapped, and the energy gained from hydrolysis is stored in a strained conformation (*19*). The N terminus of Get2 tethers the Get3/TA protein complex to the ER membrane (step 2). Binding of Get1 displaces $\alpha2^{Get2}$, and the Get3/TA protein complex is now docked to the receptor complex at the membrane (step 3). When the TA protein is released, Get3 relaxes to the closed state, and inorganic phosphate dissociates (step 4). According to the crystal structures, Get1 can stay bound to Get3 during the transition from the closed to the open state. What actually triggers opening of Get3? We favor the idea that the energy from ATP hydrolysis drives Get3 to the open state, and ADP-Mg^{2+} leaves by way of the observed tunnels. In this state, Get1 interferes with nucleotide binding and prevents closure of the dimer. Finally, binding of ATP facilitates dissociation of Get3 (step 5), which sets the stage for the next targeting cycle. As Get1-CD is rigidly linked to the TMDs, structural changes observed in the Get3/Get1 complexes can be extrapolated to the complete membrane receptor (as indicated in Fig. 4 and fig. S11). The opening of Get3 during TA protein insertion may create a force that is directly transferred to the TMDs of the receptor, which could contribute to TA protein insertion. Related structural transitions have been reported for ATP-binding cassette (ABC) transporter proteins (*27*, *28*). In Get1, the coiled-coil domain with the tip helix may have a function similar to the coupling helix in ABC transporters and may directly communicate nucleotide-dependent changes in Get3 to the transmembrane segments as anticipated in the model above. It is now important to dissect the precise mechanism of TA protein insertion and to see whether a general concept can be derived that is shared by different membrane transport systems.

References and Notes

1. G. Blobel, B. Dobberstein, *J. Cell Biol.* **67**, 835 (1975).
2. M. Schuldiner *et al.*, *Cell* **134**, 634 (2008).
3. N. Borgese, S. Brambillasca, S. Colombo, *Curr. Opin. Cell Biol.* **19**, 368 (2007).
4. B. Wattenberg, T. Lithgow, *Traffic* **2**, 66 (2001).
5. S. High, B. M. Abell, *Biochem. Soc. Trans.* **32**, 659 (2004).
6. B. C. Cross, I. Sinning, J. Luirink, S. High, *Nat. Rev. Mol. Cell Biol.* **10**, 255 (2009).
7. P. F. Egea, R. M. Stroud, P. Walter, *Curr. Opin. Struct. Biol.* **15**, 213 (2005).
8. S. O. Shan, P. Walter, *FEBS Lett.* **579**, 921 (2005).
9. A. R. Osborne, T. A. Rapoport, B. van den Berg, *Annu. Rev. Cell Dev. Biol.* **21**, 529 (2005).
10. S. Brambillasca, M. Yabal, M. Makarow, N. Borgese, *J. Cell Biol.* **175**, 767 (2006).
11. B. Meineke *et al.*, *FEBS Lett.* **582**, 855 (2008).
12. B. M. Abell, C. Rabu, P. Leznicki, J. C. Young, S. High, *J. Cell Sci.* **120**, 1743 (2007).
13. S. F. Colombo, R. Longhi, N. Borgese, *J. Cell Sci.* **122**, 2383 (2009).
14. S. Stefanovic, R. S. Hegde, *Cell* **128**, 1147 (2007).
15. V. Favaloro, F. Vilardi, R. Schlecht, M. P. Mayer, B. Dobberstein, *J. Cell Sci.* **123**, 1522 (2010).
16. C. Rabu, V. Schmid, B. Schwappach, S. High, *J. Cell Sci.* **122**, 3605 (2009).
17. V. Favaloro, M. Spasic, B. Schwappach, B. Dobberstein, *J. Cell Sci.* **121**, 1832 (2008).
18. M. Schuldiner *et al.*, *Cell* **123**, 507 (2005).
19. G. Bozkurt *et al.*, *Proc. Natl. Acad. Sci. U.S.A.* **106**, 21131 (2009).
20. A. Mateja *et al.*, *Nature* **461**, 361 (2009).
21. C. J. M. Suloway, J. W. Chartron, M. Zaslaver, W. M. Clemons Jr., *Proc. Natl. Acad. Sci. U.S.A.* **106**, 14849 (2009).
22. A. Yamagata *et al.*, *Genes Cells* **15**, 29 (2010).
23. J. Hu, J. Li, X. Qian, V. Denic, B. Sha, *PLoS ONE* **4**, e8061 (2009).
24. G. E. Tusnády, I. Simon, *Bioinformatics* **17**, 849 (2001).
25. N. Borgese, E. Fasana, *Biochim. Biophys. Acta* **1808**, 937 (2011).
26. F. Vilardi, H. Lorenz, B. Dobberstein, *J. Cell Sci.* **124**, 1301 (2011).
27. K. Hollenstein, R. J. P. Dawson, K. P. Locher, *Curr. Opin. Struct. Biol.* **17**, 412 (2007).
28. J. Zaitseva *et al.*, *EMBO J.* **25**, 3432 (2006).

Acknowledgments: V.D. would like to thank M. Frech for his support of the project and acknowledges funding by the *Deutsche Forschungsgemeinschaft* (DFG) (SFB 807), the Centre for Biomolecular Magnetic Resonance (BMRZ), and the Cluster of Excellence Frankfurt (Macromolecular Complexes). I.S. thanks J. Kopp und C. Siegmann from the crystallization platform of the Biochemiezentrum and the Cluster of Excellence Heidelberg (CellNetworks), the European Synchrotron Radiation Facility for access to data collection, B. Dobberstein for generous support and stimulating discussions, and acknowledges funding by the DFG (SFB 638). Coordinates and structure factors have been deposited in the *Research Collaboratory for Structural Bioinformatics* Protein Data Bank (PDB) with accession nos. 3SJA, 3SJB, 3SJC, and 3SJD.

Supporting Online Material

www.sciencemag.org/cgi/content/full/science.1207125/DC1
Materials and Methods
Figs. S1 to S13
Tables S1 and S2
References

18 April 2011; accepted 21 June 2011
Published online 30 June 2011;
10.1126/science.1207125

The Plant Cell Wall–Decomposing Machinery Underlies the Functional Diversity of Forest Fungi

Daniel C. Eastwood,[1]*† Dimitrios Floudas,[2]* Manfred Binder,[2]* Andrzej Majcherczyk,[3]* Patrick Schneider,[4]* Andrea Aerts,[5] Fred O. Asiegbu,[6] Scott E. Baker,[7] Kerrie Barry,[5] Mika Bendiksby,[8] Melanie Blumentritt,[9] Pedro M. Coutinho,[10] Dan Cullen,[11] Ronald P. de Vries,[12] Allen Gathman,[13] Barry Goodell,[9,14] Bernard Henrissat,[10] Katarina Ihrmark,[15] Hävard Kauserud,[16] Annegret Kohler,[17] Kurt LaButti,[5] Alla Lapidus,[5] José L. Lavin,[18] Yong-Hwan Lee,[19] Erika Lindquist,[5] Walt Lilly,[13] Susan Lucas,[5] Emmanuelle Morin,[17] Claude Murat,[17] José A. Oguiza,[18] Jongsun Park,[19] Antonio G. Pisabarro,[18] Robert Riley,[5] Anna Rosling,[15] Asaf Salamov,[5] Olaf Schmidt,[20] Jeremy Schmutz,[5] Inger Skrede,[16] Jan Stenlid,[15] Ad Wiebenga,[12] Xinfeng Xie,[9] Ursula Kües,[3]* David S. Hibbett,[2]* Dirk Hoffmeister,[4]* Nils Högberg,[15]* Francis Martin,[17]* Igor V. Grigoriev,[5]* Sarah C. Watkinson[21]*

Brown rot decay removes cellulose and hemicellulose from wood—residual lignin contributing up to 30% of forest soil carbon—and is derived from an ancestral white rot saprotrophy in which both lignin and cellulose are decomposed. Comparative and functional genomics of the "dry rot" fungus *Serpula lacrymans*, derived from forest ancestors, demonstrated that the evolution of both ectomycorrhizal biotrophy and brown rot saprotrophy were accompanied by reductions and losses in specific protein families, suggesting adaptation to an intercellular interaction with plant tissue. Transcriptome and proteome analysis also identified differences in wood decomposition in *S. lacrymans* relative to the brown rot *Postia placenta*. Furthermore, fungal nutritional mode diversification suggests that the boreal forest biome originated via genetic coevolution of above- and below-ground biota.

Many Agaricomycete fungi have been sequenced to date (*1*), permitting comparative and functional genomic analyses of nutritional niche adaptation in the underground fungal networks that sustain boreal, temperate, and some subtropical forests (*2*). Through the sequencing of the brown rot wood decay fungus *Serpula lacrymans*, we conducted genome comparisons with sequenced fungi, including species representing each of a range of functional niches: brown rot and white rot wood decay, parasitism, and mutualistic ectomycorrhizal symbiosis.

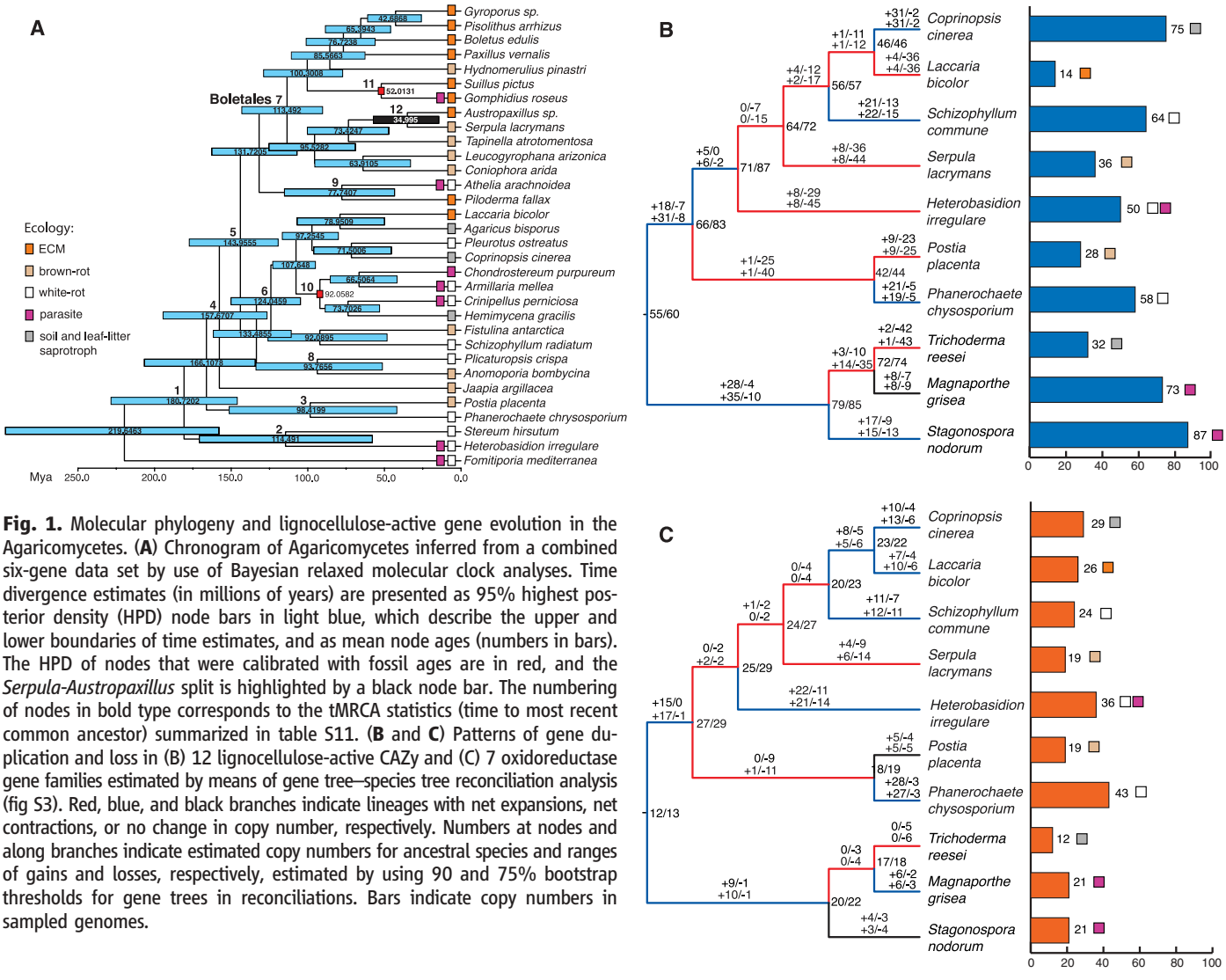

Fig. 1. Molecular phylogeny and lignocellulose-active gene evolution in the Agaricomycetes. (**A**) Chronogram of Agaricomycetes inferred from a combined six-gene data set by use of Bayesian relaxed molecular clock analyses. Time divergence estimates (in millions of years) are presented as 95% highest posterior density (HPD) node bars in light blue, which describe the upper and lower boundaries of time estimates, and as mean node ages (numbers in bars). The HPD of nodes that were calibrated with fossil ages are in red, and the *Serpula-Austropaxillus* split is highlighted by a black node bar. The numbering of nodes in bold type corresponds to the tMRCA statistics (time to most recent common ancestor) summarized in table S11. (**B** and **C**) Patterns of gene duplication and loss in (B) 12 lignocellulose-active CAZy and (C) 7 oxidoreductase gene families estimated by means of gene tree–species tree reconciliation analysis (fig S3). Red, blue, and black branches indicate lineages with net expansions, net contractions, or no change in copy number, respectively. Numbers at nodes and along branches indicate estimated copy numbers for ancestral species and ranges of gains and losses, respectively, estimated by using 90 and 75% bootstrap thresholds for gene trees in reconciliations. Bars indicate copy numbers in sampled genomes.

Only 6% of wood-decay species are brown rots (*3*), but being associated with conifer wood (*4*), they dominate decomposition in boreal forests. Their lignin residues contribute up to 30% of carbon in the organic soil horizons (*5*). Long-lived (*6*) and with capacity to bind nitrogen and cations (*7*), these phenolic polymers condition the nutrient-poor acidic soils of northern conifer forests.

Brown rot wood decay involves an initial non-enzymic attack on the wood cell wall (*8*), generating hydroxyl radicals (·OH) extracellularly via the Fenton reaction:

$$Fe^{2+} + H_2O_2 + H^+ \rightarrow Fe^{3+} + {\cdot}OH + H_2O$$

Hydrogen peroxide is metabolically generated by oxidase enzymes such as glyoxal oxidases and copper radical oxidases. The hydroxyl radical has a half-life of nanoseconds (*8*) and is the most powerful oxidizing agent of living cells. However, we do not know how it is spatially and temporally targeted to wood cell wall components. Divalent iron is scarce in aerobic environments, where the fungus is obligate and the trivalent ion is energetically favored. Phenolates synthesized by brown rot fungi, including *S. lacrymans* (*9*), can reduce Fe^{3+} to Fe^{2+}. Such phenolates may be modified lignin derivatives or fungal metabolites (*10*). After initial bond breakages in the cellulose chain, side chain hemicelluloses (arabinan and galactan) are removed, followed by main chains [xylan and mannan (*11*)], with subsequent hydrolysis of cellulose by synergistic glycoside hydrolases

[1]College of Science, University of Swansea, Singleton Park, Swansea SA2 8PP, UK. [2]Department of Biology, Clark University, Worcester, MA 01610, USA. [3]Georg-August-University Göttingen, Büsgen-Institute, Büsgenweg 2, 37077 Göttingen, Germany. [4]Friedrich-Schiller-Universität, Hans-Knöll-Institute, Beutenbergstrasse 11a, 07745 Jena, Germany. [5]U.S. Department of Energy Joint Genome Institute, Walnut Creek, CA 94598, USA. [6]Department of Forest Sciences, Box 27, University of Helsinki, Helsinki 00014, Finland. [7]Pacific Northwest National Laboratory, 902 Battelle Boulevard, Post Office Box 999, MSIN P8-60, Richland, WA 99352, USA. [8]Natural History Museum, University of Oslo, Post Office Box 1172, Blindern, NO-0138, Norway. [9]Wood Science and Technology, University of Maine, Orono, ME 04469–5755, USA. [10]UMR 6098 CNRS–Universités Aix-Marseille I and II, 13288 Marseille Cedex 9, France. [11]Forest Products Laboratory, Madison, WI 53726, USA. [12]Centraalbureau voor Schimmelcultures–Royal Netherlands Academy of Arts and Sciences Fungal Biodiversity Centre, Uppsalalaan 8, 3584 CT Utrecht, Netherlands. [13]Department of Biology, Southeast Missouri State University, Cape Girardeau, MO 63701, USA. [14]Department of Wood Science and Forest Products, 230 Cheatham Hall, Virginia Tech, Blacksburg, VA 24061, USA. [15]Department of Forest Mycology and Pathology, Swedish University of Agricultural Sciences, S-750 07 Uppsala, Sweden. [16]Department of Biology, University of Oslo, Post Office Box 1066 Blindern, N-0316 Oslo, Norway. [17]UMR 1136, Institut National de la Recherche Agronomique (INRA)–Nancy Université, Interactions Arbres/Microorganismes, INRA-Nancy, 54280 Champenoux, France. [18]Department of Agrarian Production, Public University of Navarre, 31006 Pamplona, Spain. [19]Department of Agricultural Biotechnology, Seoul National University, Seoul 151*921, Korea. [20]Department of Wood Biology, University of Hamburg, Leuschnerstrasse 91, D-21031 Hamburg, Germany. [21]Department of Plant Sciences, University of Oxford, Oxford OX1 3RB, UK.

*These authors contributed equally to this work.
†To whom correspondence should be addressed. E-mail: d.c.eastwood@swansea.ac.uk

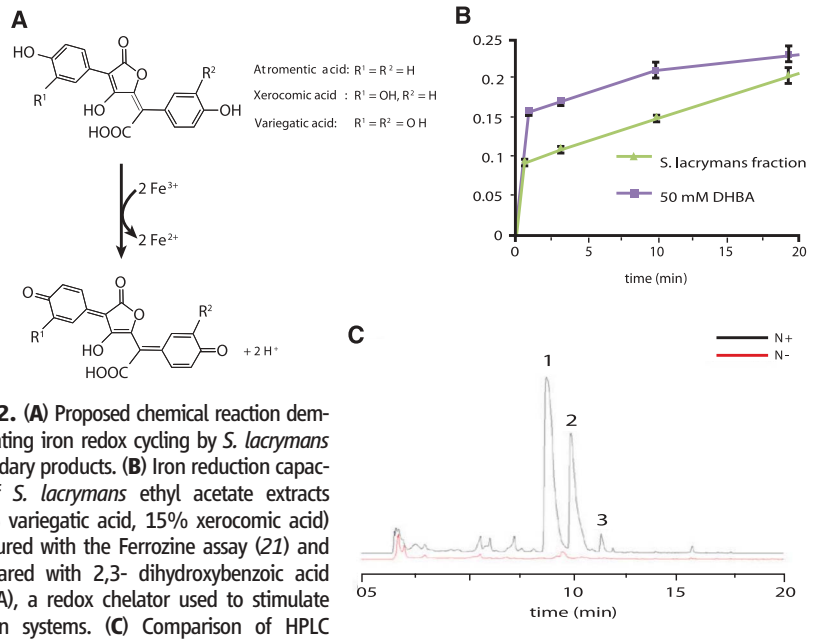

Fig. 2. (**A**) Proposed chemical reaction demonstrating iron redox cycling by *S. lacrymans* secondary products. (**B**) Iron reduction capacity of *S. lacrymans* ethyl acetate extracts (60% variegatic acid, 15% xerocomic acid) measured with the Ferrozine assay (*21*) and compared with 2,3- dihydroxybenzoic acid (DHBA), a redox chelator used to stimulate Fenton systems. (**C**) Comparison of HPLC chromatograms of *S. lacrymans* ethyl acetate extracts as a function of nitrogen supply. Red trace, nitrogen rich medium (+N); black trace, nitrogen-depleted minimal medium (–N). The identity of the compounds was confirmed with mass spectrometry and by their ultraviolet-visual spectrum (1, variegatic acid; 2, xerocomic acid; 3, atromentic acid).

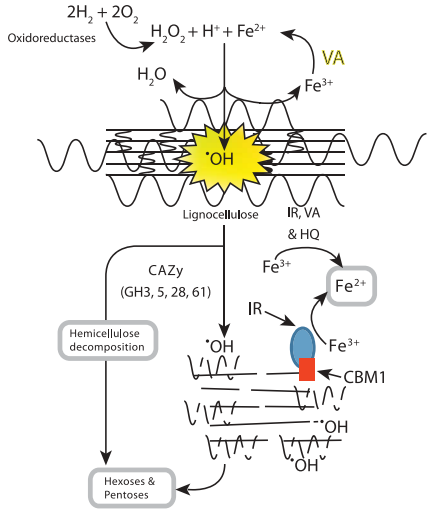

Fig. 3. Schematic overview of the proposed mechanism of wood decay by *S. lacrymans*. Scavenging mycelium colonizes a new food source, inducing VA production and expression of oxidoreductase enzymes, which drive hydroxyl radical attack on the lignocellulose composite. CAZy gain access to the weakened composite structure and break down accessable carbohydrates. Cellulose-binding iron reductase targets ·OH-generating Fenton's reaction on cellulose chains, releasing chain ends for hydrolysis and assimilation. IR, iron reductase; HQ, hydroxyquinones; CBM, cellulose-binding module.

(GHs). Residual lignin is demethylated. In contrast, white rot fungi decompose both cellulose and lignin, with free radical attack theorized to break a variety of bonds in the lignin phenylpropanoid heteropolymer.

S. lacrymans is in the Boletales, along with several ectomycorrhizal lineages (Fig. 1A) (*12*). *S. lacrymans* is thus phylogenetically distant from brown rot *Postia placenta* (*Polyporales*) (*13*), as well as other sequenced ectomycorrhizal fungi (*14*, *15*), parasites, and white rot wood decomposers (*16*). We estimated divergence dates in fungal phylogeny using the data set of Binder *et al.* [supporting online material (SOM), molecular clock analyses] (*17*), with two well-characterized fungal fossils that were used to calibrate the minimum ages of the marasmioid (Fig. 1A, node 10) and suilloid clades (Fig. 1A, node 11). The estimated age of the split between *Serpula* and its ectomycorrhizal sister-group *Austropaxillus* (53.1 to 15 million years ago) (Fig. 1A and table S11) suggests that transition from brown rot saprotrophy to mutualistic symbiosis occurred after rosids (Eurosids I) became widespread (Fig. 1A) (*18*). Diversification in fungal nutritional modes occurred alongside diversification of angiosperms and gymnosperms, as these fungi are currently associated with members of both gymnosperms (Pinaceae) and angiosperms (*18*).

S. lacrymans comprises two subgroups that diverged in historic time (*19*), *S. lacrymans* var. *shastensis*, which is found in montane conifer forest, and *S. lacrymans* var. *lacrymans*, which is a cause of building dry rot. Two *S. lacrymans* var. *lacrymans* complementary monokaryons (haploids of strain S7), S7.9 (A2B2) and S7.3 (A1B1) (*20*), were sequenced via Sanger and 454 pyrosequencing, respectively. The genome of *S. lacrymans* S7.9 was 42.8 megabase pairs (Mbp), containing 12,917 gene predictions (*21*).

We analyzed 19 gene families of enzymes for lignocellulose breakdown: carbohydrate active enzymes (CAZys; www.cazy.org) (*22*) (GHs and carbohydrate esterases) and oxidoreductases (table S9). Losses and expansions in these families were compared across 10 fungi, including Agaricomycetes, with a range of nutritional modes (Fig. 1, B and C, and table S9). Convergent changes in enzyme complement were found in the two independently evolved brown rot species, with parallels in the ectomycorrhizal *Laccaria bicolor* (fig. S3 and table S9). The inferred most recent common ancestor of the Agaricales, Boletales, and Polyporales is predicted to be a white rot with 66 to 83 hydrolytic CAZy genes and 27 to 29 oxidoreductases (Fig. 1, B and C). Brown rot and ectomycorrhizal fungi have the fewest hydrolytic CAZy genes. Brown rot fungi have the fewest oxidoreductases, not because of gene losses but because of gene duplications in white rot species.

Both brown rot and ectomycorrhizal fungi lacked class II peroxidases, which are used by white rot fungi in depolymerizing the lignin matrix of wood and unmasking usable cellulose embedded within it. This family was expanded in the white rots *Coprinopsis cinerea*, *Phanerochaete chrysosporium*, and *Schizophyllum commune*, with 29, 43, and 24 genes, respectively, with only 19 each in *S. lacrymans* and *P. placenta*. Oxidoreductases conserved in brown rot fungi included iron and quinone reductases and multicopper oxidases (fig. S3 and table S8). Absence of ligninolysis in brown rots raises the question of how they achieve pervasive cellulolysis in wood with the lignin matrix intact.

GH gene families had parallel patterns of losses and expansion in both brown rots and ectomycorrhizas. CAZy families GH5 (endoglucanases, hydrolyzing cellulose) and GH28 (pectinases, hydrolyzing intercellular cohesive polysaccharides in plant tissues) were expanded in both brown rot species, in which they might facilitate intercellular enzyme diffusion, and retained in *L. bicolor*, in which they might facilitate intercellular penetration of living roots. Both brown rot species lacked GH7 (endoglucanase/cellobiohydrolase CBHI), and GH61 genes—with unknown function but recently implicated in oxidative attack on polysaccharides (*23*)—were reduced. GH6 (cellobiohydrolase CBHII) and cellulose-binding modules (CBM1), which were absent from *P. placenta* (*13*), were present in *S. lacrymans*. One CBM was associated with an iron reductase in a gene (*S. lacrymans* S7.9 database protein ID, 452187) originally derived from a cellobiose dehydrogenase (fig. S5).

The general utility of the conserved suite of GH genes in wood decay by *S. lacrymans* was supported through transcriptomic and proteomic analysis. Carbohydrate-active enzymes accounted for 50% of proteins identified (table S14), and 33.9% of transcripts regulated greater than 20-fold by *S. lacrymans* growing on pine wood as compared with glucose medium (fig. S4).

Cellulose-, pectin-, and hemicellulose-degrading enzymes (GH families 5, 61, 3, and 28) were prominent, and GH5 endoglucanase (*S. lacrymans* S7.9 database protein ID, 433209) and GH74 endoglucanase/xyloglucanase (*S. lacrymans* S7.9 database protein ID, 453342) were up-regulated greater than 100-fold.

We conclude that brown rot fungi have cast off the energetically expensive apparatus of ligninolysis and acquired alternative mechanisms of initial attack. Wood decomposition by *S. lacrymans* may involve metabolically driven nonenzymatic disruption of lignocellulose with internal breakage of cellulose chains by highly localized ·OH radical action. Mycelia in split plates mimicking realistic nutrient heterogeneity (fig. S1) produced variegatic acid (VA), an iron-reducing phenolate (Fig. 2, A to C), via the Boletales atromentin pathway, which was recruited in *S. lacrymans* for the Fenton's reaction. The genome was rich in secondary metabolism genes (table S15), including a putative atromentin locus (*24*). Mycelium imports amino acids to sites of wood colonization (*25*), which is consistent with observed up-regulation of oligopeptide transporters on wood (table S12). Localizing variegatic acid production to well-resourced parts of the mycelium could enhance Fenton's chemistry in contact with wood.

Wood colonization is presumably followed by coordinated induction of the decay machinery revealed in the wood-induced transcriptome (Fig. 3 and fig. S4). GHs and oxidoreductases accounted for 20.7% of transcripts, accumulating greater than fourfold on wood relative to glucose medium (fig. S4 and table S12). Iron reduction mechanisms included an enzyme harboring a C terminal cellulose-binding module (*S. lacrymans* S7.9 database protein ID, 452187) (fig. S5) that is up-regulated 122-fold on wood substrate (fig. S4 and table S12). This enzyme, which is present in *Ph. chrysosporium* but absent from *P. placenta* (*26*), is a potential docking mechanism for localizing iron reductase activity, and hence ·OH generation, on the surface of microcrystalline cellulose. Cellulose-targeted iron reduction, combined with substrate induction of variegatic acid biosynthesis, might explain the particular ability of brown rot fungi in Boletales to degrade unassociated microcrystalline cellulose without the presence of lignin (*27*).

Thus, comparative genomics helps us understand the molecular processes of forest soil fungi that drive the element cycles of forest biomes (*28*). Sequenced forest Agaricomycetes revealed shared patterns of gene family contractions and expansions associated with emergences of both brown rot saprotrophy and ectomycorrhizal symbiosis. In Boletales, loss of aggressive ligninolysis might have permitted brown rot transitions to biotrophic ectomycorrhiza, which is promoted in soils impoverished in nitrogen by brown rot residues, and by the nutritional advantage conferred by the connection to a mycorrhizal network. *S. lacrymans* and other fungi cultured with conifer roots (*29*) ensheath *Pinus sylvestris* roots with a mantle-like layer (fig. S6), suggesting nutrient exchange.

The chronology of divergences in extant fungal nutritional mode (Fig. 1A) matches the predicted major diversification in conifers (*18*), suggesting that the boreal forest biome may have originated via genetic coevolution of above- and belowground biota.

References and Notes

1. F. Martin *et al.*, *New Phytol.* **190**, 818 (2011).
2. F. Martin, in *Biology of the Fungal Cell*, R. J. Howard, N. A. R. Gow, Eds. (Springer Berlin, Heidelberg, 2007), vol. 8, pp. 291–308.
3. R. L. Gilbertson, *Mycologia* **72**, 1 (1980).
4. D. S. Hibbett, M. J. Donoghue, *Syst. Biol.* **50**, 215 (2001).
5. K.-E. Eriksson, R. A. Blanchette, P. Ander, *Microbial and enzymatic degradation of wood and wood components* (Springer-Verlag, Berlin, New York, 1990).
6. B. D. Lindahl *et al.*, *New Phytol.* **173**, 611 (2007).
7. R. R. Northup, Z. Yu, R. A. Dahlgren, K. A. Vogt, *Nature* **377**, 227 (1995).
8. B. Goodell *et al.*, *J. Biotechnol.* **53**, 133 (1997).
9. T. Shimokawa, M. Nakamura, N. Hayashi, M. Ishihara, *Holzforschung* **58**, 305 (2005).
10. V. Arantes, A. M. Milagres, T. R. Filley, B. Goodell, *J. Ind. Microbiol. Biotechnol.* **38**, 541 (2011).
11. S. F. Curling, C. A. Clausen, J. E. Winandy, *Int. Biodeterior. Biodegradation* **49**, 13 (2002).
12. M. Binder, D. S. Hibbett, *Mycologia* **98**, 971 (2006).
13. D. Martinez *et al.*, *Proc. Natl. Acad. Sci. U.S.A.* **106**, 1954 (2009).
14. F. Martin *et al.*, *Nature* **464**, 1033 (2010).
15. F. Martin *et al.*, *Nature* **452**, 88 (2008).
16. D. Martinez *et al.*, *Nat. Biotechnol.* **22**, 695 (2004).
17. M. Binder, K. H. Larsson, P. B. Matheny, D. S. Hibbett, *Mycologia* **102**, 865 (2010).
18. A. J. Eckert, B. D. Hall, *Mol. Phylogenet. Evol.* **40**, 166 (2006).
19. H. Kauserud *et al.*, *Mol. Ecol.* **16**, 3350 (2007).
20. O. Schmidt, *Holzforschung* **54**, 221 (2000).
21. Materials and methods are available as supporting material on *Science* Online.
22. B. L. Cantarel *et al.*, *Nucleic Acids Res.* **37**, D233 (2009).
23. G. Vaaje-Kolstad *et al.*, *Science* **330**, 219 (2010).
24. P. Schneider, S. Bouhired, D. Hoffmeister, *Fungal Genet. Biol.* **45**, 1487 (2008).
25. M. Tlalka, M. Fricker, S. Watkinson, *Appl. Environ. Microbiol.* **74**, 2700 (2008).
26. A. Vanden Wymelenberg *et al.*, *Appl. Environ. Microbiol.* **76**, 3599 (2010).
27. T. Nilsson, J. Ginns, *Mycologia* **71**, 170 (1979).
28. B. O. Lindahl, A. F. S. Taylor, R. D. Finlay, *Plant Soil* **242**, 123 (2002).
29. R. Vasiliauskas, A. Menkis, R. D. Finlay, J. Stenlid, *New Phytol.* **174**, 441 (2007).

Acknowledgments: J. Schilling, University of Minnesota, and D. Barbara, University of Warwick, critically reviewed the manuscript; T. Marks designed graphics; and B. Wackler and M. Zomorrodi gave technical assistance. Assembly and annotations of *S. lacrymans* genomes are available at www.jgi.doe.gov/Serpula and DNA Data Bank of Japan/European Molecular Biology Laboratory/GenBank, accessions nos. AECQB00000000 and AEQC00000000. The complete microarray expression data set is available at the Gene Expression Omnibus (www.ncbi.nlm.nih.gov/geo/) accession no. GSE27839. The work was conducted by the U.S. Department of Energy Joint Genome Institute and supported by the Office of Science of the U.S. Department of Energy under contract DE-AC02-05CH11231. Further financial support is acknowledged in the supporting online material on *Science* Online.

Supporting Online Material

www.sciencemag.org/cgi/content/full/science.1205411/DC1
Materials and Methods
SOM Text
Figs. S1 to S6
Tables S1 to S15
References (*30*–*89*)

10 March 2011; accepted 20 June 2011
Published online 14 July 2011;
10.1126/science.1205411

The Leukemogenicity of AML1-ETO Is Dependent on Site-Specific Lysine Acetylation

Lan Wang,[1] Alexander Gural,[1] Xiao-Jian Sun,[2] Xinyang Zhao,[1] Fabiana Perna,[1] Gang Huang,[1] Megan A. Hatlen,[1] Ly Vu,[1] Fan Liu,[1] Haiming Xu,[1] Takashi Asai,[1] Hao Xu,[1] Tony Deblasio,[1] Silvia Menendez,[1] Francesca Voza,[1] Yanwen Jiang,[3] Philip A. Cole,[4] Jinsong Zhang,[5] Ari Melnick,[3] Robert G. Roeder,[2] Stephen D. Nimer[1]*

The chromosomal translocations found in acute myelogenous leukemia (AML) generate oncogenic fusion transcription factors with aberrant transcriptional regulatory properties. Although therapeutic targeting of most leukemia fusion proteins remains elusive, the posttranslational modifications that control their function could be targetable. We found that AML1-ETO, the fusion protein generated by the t(8;21) translocation, is acetylated by the transcriptional coactivator p300 in leukemia cells isolated from t(8;21) AML patients, and that this acetylation is essential for its self-renewal–promoting effects in human cord blood CD34$^+$ cells and its leukemogenicity in mouse models. Inhibition of p300 abrogates the acetylation of AML1-ETO and impairs its ability to promote leukemic transformation. Thus, lysine acetyltransferases represent a potential therapeutic target in AML.

Histone-modifying enzymes can regulate the binding of specific chromatin-binding proteins to histone marks and can change the affinity of the histones for DNA (*1*, *2*). These enzymes also affect nonhistone proteins, and posttranslational modifications of transcription factors such as p53 or AML1 (which is required for definitive hematopoietic development) can

ERRATUM

Post date 30 September 2011

Reports: "The plant cell wall–decomposing machinery underlies the functional diversity of forest fungi" by D. C. Eastwood *et al.* (5 August, p. 762). The second sentence of the caption for Fig. 2C should read, "Black trace, nitrogen-rich medium (+N); red trace, nitrogen-depleted minimal medium (–N)."

The Plant Cell Wall–Decomposing Machinery Underlies the Functional Diversity of Forest Fungi

Daniel C. Eastwood, Dimitrios Floudas, Manfred Binder, Andrzej Majcherczyk, Patrick Schneider, Andrea Aerts, Fred O. Asiegbu, Scott E. Baker, Kerrie Barry, Mika Bendiksby, Melanie Blumentritt, Pedro M. Coutinho, Dan Cullen, Ronald P. de Vries, Allen Gathman, Barry Goodell, Bernard Henrissat, Katarina Ihrmark, Hävard Kauserud, Annegret Kohler, Kurt LaButti, Alla Lapidus, José L. Lavin, Yong-Hwan Lee, Erika Lindquist, Walt Lilly, Susan Lucas, Emmanuelle Morin, Claude Murat, José A. Oguiza, Jongsun Park, Antonio G. Pisabarro, Robert Riley, Anna Rosling, Asaf Salamov, Olaf Schmidt, Jeremy Schmutz, Inger Skrede, Jan Stenlid, Ad Wiebenga, Xinfeng Xie, Ursula Kües, David S. Hibbett, Dirk Hoffmeister, Nils Högberg, Francis Martin, Igor V. Grigoriev and Sarah C. Watkinson

Science **333** (6043), 762-765.
DOI: 10.1126/science.1205411originally published online July 14, 2011